Journal of Marine Research, 73, 207–232, 2015

The wall-layer dynamics in a weakly stratified tidal bottom boundary layer

by I. Lozovatsky[1,2], S. U. P. Jinadasa[3], H. J. S. Fernando[1,4], J.-H. Lee[5], and Chang Su Hong[5]

ABSTRACT

The application of the classical logarithmic layer model for wall-bounded shear flows to marine bottom boundary layer (BBL) usually leads to an overestimation of the friction velocity u_* due possibly to the influence of form drag, stratification, and rotation of the flow vector. To gain insights on the BBL velocity scaling, acoustic Doppler current profiler (ADCP) measurements taken in the East China Sea were analyzed (a total of 270 sixteen-minute averaged velocity profiles). Single and double log-layer models, a log-wake model, and a modified log-layer (MLL) model that accounts for stratification in the upper part of the BBL (Perlin, Moum, Klymak, Levine et al. 2005) were explored. Although the first three models fit well for a majority of the profiles, the friction velocities appeared to be substantially overestimated, leading to unreasonably high drag coefficients. The friction velocity u_{*ml} inferred from a slightly modified MLL, however, is half of that estimated using the classical log-layer assumption u_{*l}. In a weakly stratified extended BBL, the dissipation rate ε decreases with the height from the seafloor ζ much faster than that in a homogeneous stationary BBL. This observation could be well approximated (in terms of r^2) by an exponential $\varepsilon(\zeta) = \varepsilon_0 e^{-\zeta/L_m}$ or a power law decrease. The mixing length scale $L_m = c_L h_{BL}$, where $h_{BL} = 19$–20 m is the BBL height and $c_L = 0.17$, as well as the characteristic dissipation ε_0, should vary in time, depending on the tidal currents and stratification in the BBL. The eddy diffusivity $K_N = 0.2\varepsilon/N^2$ showed an inverse dependence on the Richardson number Ri according to $K_N = K_0/(1 + Ri/R_c)$, where R_c is a constant and the diffusivity in nonstratified flow near the seafloor $K_0 = u_*\kappa\zeta$ is specified using $u_* = u_{*ml}$.

Keywords: Turbulence, bottom boundary layer, logarithmic velocity profile, friction velocity, tidal flow, diffusivity

1. Environmental Fluid Dynamics Laboratories, Department of Civil and Environmental Engineering and Earth Sciences, University of Notre Dame, Notre Dame, IN 46556.
2. Corresponding author: ***e-mail: i.lozovatsky@nd.edu***
3. National Aquatic Resources Research and Development Agency, Crow Island, 15 Colombo, Sri Lanka.
4. Department of Aerospace and Mechanical Engineering, University of Notre Dame, Notre Dame, IN 46556.
5. Korean Institute of Ocean Science and Technology, 787 Haean-ro(st), Sangnok-gu, Ansans-si, Gyeonggi-do, 426-744, Korea.

1. Introduction

The classical logarithmic velocity profile,

$$U(\zeta) = \frac{u_*}{\kappa} \ln \frac{\zeta}{\zeta_0}, \tag{1}$$

is valid for a steady, fully developed, and nonstratified parallel shear flow with a constant shear stress τ_s near a solid boundary; here $U(\zeta)$ is the velocity amplitude at a distance ζ from the boundary, $u_* = \sqrt{\tau_s/\rho}$ is the friction velocity, ζ_0 is the aerodynamic roughness (which is not the physical roughness), and κ is the von Karman constant (e.g., Schlichting 1968). Application of equation (1) to the oceanic bottom boundary layer (BBL) usually leads to an overestimation of the friction velocity, possibly contributed by the form drag (Sanford and Lien 1999), stratification (Perlin et al. 2005), and rotation of the flow vector (Lozovatsky et al. 2008b; Sakamoto and Akitomo 2008; Yoshikawa et al. 2010). The BBL in stratified shallow seas, as in the East China Sea (ECS) in the summertime, extends from the seafloor to the outer free flow up to 15–25 m above the bottom (mab), being separated from the overlying stratified waters by a distinct density interface (Lozovatsky et al. 2008a). Although the BBL is fairly well mixed, stratification inside the layer may gradually increase from a narrow, almost completely mixed sublayer near the seafloor toward the water interior. As the result, the thickness of the homogeneous BBL sometimes may not be clearly identified. The BBL thickness is mainly governed by the shear of the mean flow, ambient stratification (buoyancy frequency), rotation (the Coriolis and possibly tidal frequencies) and the bottom roughness. In shallow waters, the BBL dynamics can also be influenced by winds (Grant and Madsen 1986), surface (e.g., Burchard et al. 2008) and internal (Thorpe 2005) waves, and horizontal advection especially over sloping bottom (e.g., Trowbridge and Lentz 1991; Cyr, Bourgault, and Galbraith 2011, 2015). The characteristics of the BBL turbulence in the ECS such as the kinetic energy dissipation rate and friction velocity have been reported (Lozovatsky et al. 2008b; Yoshikawa et al. 2010; Lozovatsky et al. 2012), and intermittency of near-bottom ($\zeta = 1$ mab) turbulence has been analyzed by Lozovatsky et al. (2010) using high spatial resolution measurements.

The data from upward-looking bottom-mounted acoustic Doppler current profilers (ADCPs) confirmed that the log-layer approximation to the velocity profile in the BBL may be applicable for shallow waters when the BBL is well mixed (Gross and Nowell 1983; Lueck and Lu 1997; Foster, Beach, and Holman 2000; Elliott 2002; Howarth and Souza 2005; Lozovatsky et al. 2008a, 2008b). Velocity profiles in the BBL above the viscous sublayer/roughness elements, however, often deviate from equation (1), which has been attributed to the violation of assumptions underlying equation (1). Such observations predate the ADCP era (e.g., Chriss and Caldwell 1982; Grant and Madsen 1986; Johnson, Lueck, and Sanford 1994). Notwithstanding that BBL currents are usually subjected to weak stratification and often to rotation (if the BBL is not very shallow; e.g., Perlin et al. 2007; Sakamoto and Akitomo 2008), the measured $U(\zeta)$ profiles have often been approximated by equation (1) in order to deduce u_* without paying much attention to the

prevailing conditions. Unsurprisingly, significant overestimations of u_* have been noted not only for oceanic (e.g., Sanford and Lien 1999) but also atmospheric stratified boundary layers, where u_* dependence on stability has been observed (Leo et al. 2015). This is an important issue, specifically for shallow basins with strong stratification during the warm season, such as the ECS where our measurements have been conducted ~100 miles to the southwest of Jeju Island (Korea).

The observational setup, data, background stratification, and turbulence profiles in the study area are given in Section 2. In Section 3, the vertical structure of BBL currents $U(\zeta)$ is analyzed. Sections 3a and 3b are focused on single and double log-layer approximations and corresponding estimates of the friction velocity u_{*l}. A log-wake model (Coles 1956) of $U(\zeta)$ is explored in Section 3c, and the influence of stratification on $U(\zeta)$ and consequently on u_{*ml} is analyzed in Section 3d, based on a slightly modified log-layer (MLL) model of Perlin et al. (2005). Section 3e discusses characteristic sublayers of the BBL relevant to the MLL model, and a parameterization for the BBL dissipation profiles is offered in Section 3f. Results are summarized in Section 4.

2. Measurements and data

To study the BBL dynamics of ECS, a bottom-mounted 600 kHz ADCP was set up on 13 August 2006, ~6 miles to the northeast of the Socotra Rock (32°07.23′ N, 125°10.57′ E), which is the base of the Ieodo Ocean Research Station (http://ieodo.khoa.go.kr). The tidal-averaged depth of the seafloor at the deployment site (32°11.7′ N, 125°21.12′ E) was 63 m. At the beginning of observations, stable atmospheric conditions were characterized by a low southwesterly wind of 3 m s^{-1}, which then decreased to 1–2 m s^{-1}. The sea was calm with the visual wave height estimates less than ~0.5 m. The air temperature varied from 28.2°C–28.5°C at night to 29.5°C–29.7°C during the daytime.

a. ADCP data

The bottom-mounted ADCP provided 1 m bin-averaged profiles of the velocity components $u(\zeta, t)$ and $v(\zeta, t)$ in a limited range of the water column up to $\zeta = 36.7$ mab. Because of the height of the ADCP pedestal (a circular disc of heavy cement with a central hole for mounting the instrument atop) and signal blanking near the ADCP heads, the first bin was centered at $\zeta = 3.7$ mab. The pitch and roll signals of the rigidly mounted instrument did not exceed 0.2 and 0.75 degrees, respectively, ensuring that the measured horizontal velocity components are of high quality. The records contained a small number of spikes of unknown origin, which were removed, and the gaps were interpolated during the data quality control. To analyze the variability of the velocity amplitude $U = \left(u^2 + v^2\right)^{1/2}$, 16 min bin averaging was applied to every 32 consecutive ADCP samples in every 1 m bin, which produced reliable, averaged data records at relatively stationary segments of the non-stationary tidal flow. Because the instrument operated in the "earth coordinates" mode (Lu and Lueck 1999a), registering relatively low-frequency sampled (0.033 Hz) zonal $u(\zeta, t)$

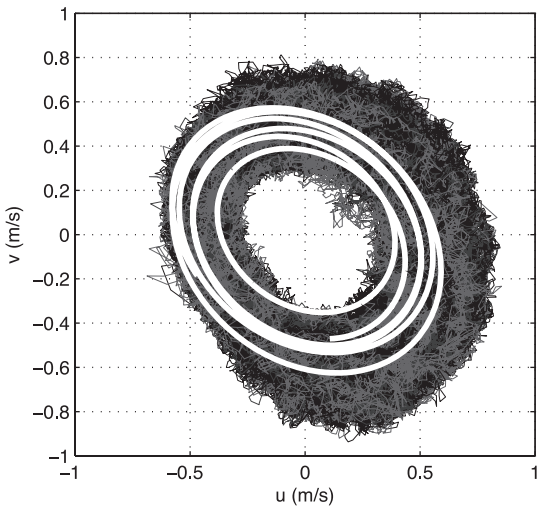

Figure 1. Hodograph of the rotating tidal flow for 13–16 August 2006. Grayscale lines are the combined acoustic Doppler current profiler (ADCP) data for all 33 ADCP bins (from $\zeta = 3.7$ to $\zeta = 36.7$ m above the bottom); white ellipses are the OTIS (Oregon State University Tidal Inversion Software, http://volkov.oce.orst.edu/tides/global.html) modeling currents using 10 major tidal constituents. The amplitudes of barotropic tidal components decreased during the observational period.

and meridional $v\,(\zeta, t)$ velocity components rather than high-frequency (typically 1–2 Hz) beam velocities, the ADCP data set obtained was not suitable for calculating turbulence characteristics such as Reynolds stresses and friction velocity using the variance method (e.g., Lu and Lueck 1999b; Stacey, Monismith, and Burau 1999). Note that the beam velocities may be obtained from u, v, and w recorded in the "earth coordinates," using an additional variable, the so-called error velocity e (van Haren, Oakey, and Garrett 1994, their equation 3), which, however, is useless for mean currents calculation and therefore was not stored after processing the original ADCP records.

The Tidal Inversion Software (Egbert and Erofeeva 2002) provided the barotropic tidal components $u_{BT}\,(t)$, $v_{BT}\,(t)$, and sea surface elevation $\xi_{BT}\,(t)$ at the site. The clockwise rotating tidal ellipses, which are close to circles (Kang et al. 2002), decreased in time (Fig. 1), indicating that the observations were conducted during the transition period from spring to neap tide. The measured currents were dominated by tidal flow (Fig. 1), with additional contributions from numerous smaller-scale dynamical processes, specifically in the sharp pycnocline ($\zeta = 25$–30 mab). The amplitudes of u_{BT} and v_{BT} decreased during the observational period from $\sim$0.6 to 0.4 m s^{-1} (Fig. 1). The surface tidal amplitude ξ_{BT} ceased from $\sim$1 to 0.7 m, when transitioning from the spring to the neap tide. Anticlockwise veering of mean currents was observed from the seafloor toward the upper boundary of BBL,

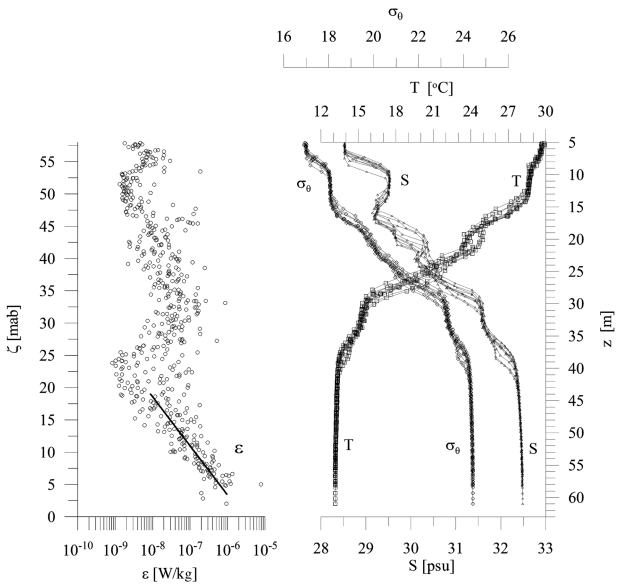

Figure 2. Temperature $T\,(z)$, salinity $S\,(z)$, potential density anomaly $\sigma_\theta\,(z)$, and the kinetic energy dissipation rate $\varepsilon\,(\zeta)$ in the vicinity of the acoustic Doppler current profiler mooring. The exponential approximation $\varepsilon\,(\zeta) = \varepsilon_0 e^{-\zeta/L_m}$ in the bottom boundary layer is shown by a heavy straight line; $\varepsilon_0 = 2.8 \times 10^{-6}$ W kg^{-1}, and $L_m = 3.3$ m.

similarly to that reported by Yoshikawa et al. (2010) in the ECS during the 2007–2009 campaigns conducted ∼52 km to the south and 208 km to the southeast from our test site.

b. TurboMap data

Profiles of temperature $T(z)$, salinity $S(z)$, potential density $\rho_\theta\,(z)$, and the kinetic energy dissipation $\varepsilon\,(z)$ with 1 m vertical averaging were obtained using TurboMAP microstructure profiler (Wolk et al. 2002) from the drifting ship, R/V *EARDO* of the Korean Institute of Ocean Science and Technology (formerly KORDI). The squared buoyancy frequency $N^2\,(z) = (g/\rho_0)\,\partial\tilde{\rho}_\theta/\partial z$, where g and ρ_0 are the gravity and reference density, respectively, was calculated based on the monotonically sorted potential density profile in each TurboMAP cast, $\tilde{\rho}_\theta\,(z)$, with z positive downward. In this study, the TurboMAP data obtained within a 1.5 h time interval when the ship drifted ∼2 km to the north from the ADCP mooring location are examined. The corresponding $T(z)$, $S(z)$, and potential density anomaly $\sigma_\theta\,(z)$ profiles (Fig. 2) depict a thick BBL below z ∼42–43 m, which is topped by a sharp and richly layered thermohalocline ($\Delta T \approx 15$°C, $\Delta S \approx 4$ psu in the depth range $\sim 40 < z < \sim 15$ m). A subsurface mixed layer possibly of intrusive origin was embedded ($\sim 9 < z < \sim 14$ m) in the diurnal pycnocline of very warm, diluted water.

The processing of microstructure data and calculation of ε followed those of Roget et al. (2006). The accuracy of ε estimates is ∼50%, which is typical for microstructure profiling measurements (e.g., Wolk et al. 2002). The dissipation profiles ε (ζ) shown in Figure 2 suggest a variation of ε in the range of $\sim 10^{-6}$ to 10^{-8} W kg^{-1}, with a minimum of $\sim 10^{-9}$ W kg^{-1} near the upper boundary of BBL. Note that in the subsurface mixed layer, ε is close to its lowest values, presumably due to lack of penetration or generation of turbulence below the subsurface layer. In the BBL, the dissipation rate on average sharply decreases upward from the seafloor: at ζ = 4–5 mab, $\varepsilon_{nb} \approx 2 \times 10^{-6}$ W kg^{-1}, and at ζ = 19–21 mab, $\varepsilon_{min} \approx 10^{-9}$ W kg^{-1}. The dissipation rate ε (ζ) in stratified BBL (above ζ ∼ 4 m) does not follow the classical (Schlichting 1968) log-layer formula $\varepsilon(\zeta) = u_*^3/\kappa\zeta$. An exponential function, $\varepsilon(\zeta) = \varepsilon_0 e^{-\zeta/L_m}$, shown in Figure 2 can serve as an empirical approximation for ε (ζ) with $\varepsilon_0 = 2.8 \times 10^{-6}$ W kg^{-1}, which is a characteristic value of ε_0 for the period of the dissipation measurements, but ε_0 varies in time following mainly the magnitude of tidal currents and possible changes of the BBL stratification. The scaling factor $L_m = 3.3$ m can be interpreted as an integral scale of the BBL turbulence, which is often specified via the BBL height $\zeta = h_{BL} \sim$ 19–20 mab multiplied by a constant, $c_L = 0.1$–0.2 (e.g., Blackadar 1962). For our data set, $c_L \approx 0.17$. Cyr, Bourgault, and Galbraith (2011, 2015) examined boundary mixing above the sloping bottom in the Gulf of St. Lawrence (Canada). Although turbulent dissipation in the BBL was high (the mean $\tilde{\varepsilon} \sim 10^{-7}$ to 10^{-8} W kg^{-1}), the BBL (∼10 m thick) maintained its stratification with $N^2 > 10^{-5}$ s^{-2} (Cyr et al., 2015). These measurements showed an approximate exponential growth of ε toward the bottom (fig. 13 of Cyr, Bourgault, and Galbraith 2011). On average, $\tilde{\varepsilon}(\zeta) = \varepsilon_{oc} e^{-\zeta/2.4}$ between ζ = 3 and 8 mab; $\varepsilon_{oc} = 2.6 \times 10^{-7}$ W kg^{-1}. The parameters of the approximation are consistent with our approximation of ε (ζ) in the ECS BBL. Despite that no specific reason for exponential decay of ε (ζ) with the distance from the seafloor is offered, we can refer to several other studies (e.g., Rippeth [2005], in which the approximately exponential section of ε (ζ) is shown in his fig. 4 between ζ ∼ 5 and 20 mab, the dissipation measurements in the Irish Sea). Walter et al. (2014) analyzed the dissipation rate scaling at the various heights in the BBL of Monterey Bay and found that closer to the seabed (0.3, 1, and 2 mab), the law of the wall scaling for dissipation, $\varepsilon = u_*^3/\kappa\zeta$, typically matches the order of magnitude of the observed dissipation values (their fig. 5). Further up in the water column, however, this scaling begins to break down. The authors suggest that result is likely due to the presence of stratification that acts to modify the logarithmic region and the applicable turbulent length scales (i.e., the turbulent eddies outside of the constant-stress wall region no longer scale as the distance from the wall). The analysis of our dissipation measurements in the BBL with respect to the dependence of ε on the gradient Richardson number is given in Section 3f.

Note that the sea surface wave-induced orbital motions are negligible at the depths $z > z_w \approx 0.16 g \tau_w^2$ (linear wave theory; e.g., Souza and Friedrichs 2005). For significant wave height of ∼0.5 m, a characteristic wave period, τ_w, is ∼4–5 s (Souza and Howarth 2005). Thus, z_w is less than 25–40 m, and therefore, the BBL dynamics were not affected by surface waves.

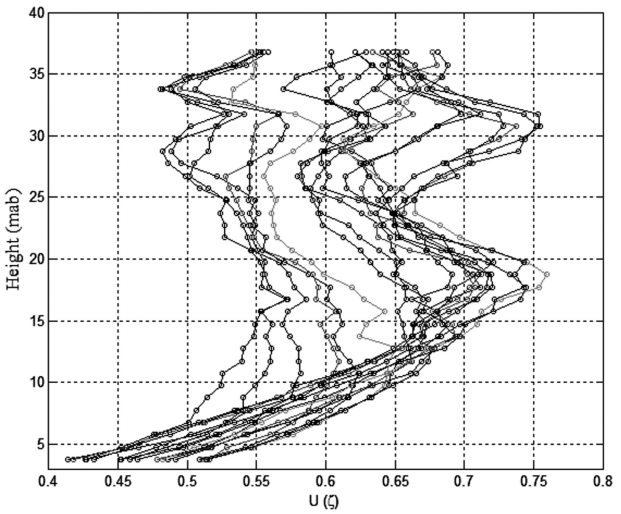

Figure 3. A series of the consecutive velocity profiles exemplifying tidal-induced variability of the height of a seemingly logarithmic near-bottom layer, which ranges in this plot between 7 and 20 m above the bottom (mab).

3. Results and discussion

a. Classic log-layer approximation

i. The log-layer height. It has been shown (Lozovatsky et al. 2008b, 2012) that velocity profiles near the bottom in rotating tidal flows of ECS often accord with equation (1) over 10–15 min time intervals, although the reliability of equation (1) for estimating u_* and ζ_0 is still in question.

During 70 h of our ADCP measurements, 270 bin-averaged velocity profiles $U(\zeta, t)$ were obtained; the evolution of several individual averaged profiles is exemplified in Figure 3. It appears that, starting from the first bin ($\zeta = 3.7$ mab), equation (1) can be fitted to all velocity profiles at segments of different length (see typical example in Fig. 4a). Moreover, 69 out of 270 profiles exhibited a secondary log-layer segment, just above the first one (see example in Fig. 4c). The coefficient of determination for the first (lowest) log layer exceeded $r^2 > 0.94$, and for the secondary log layer, $r^2 > 0.97$. The cumulative distribution functions of r^2 for fitting equation (1) to the data are shown in Figure 5 for both classic log layers and the MLL (equation 5) discussed subsequently.

The upper boundary or the first logarithmic layer $h_{l1}(t)$ varies in the range of 5.7–21.7 mab (Fig. 6) driven mainly by higher harmonics of semidiurnal tidal flow. The most recognizable periods of ∼4 and 6 h were also identified in spectral densities of velocity components (not shown here). A characteristic height of the logarithmic layers reported by Lueck and Lu (1997), Sanford and Lien (1999), and Lozovatsky et al. (2008a) for shallow

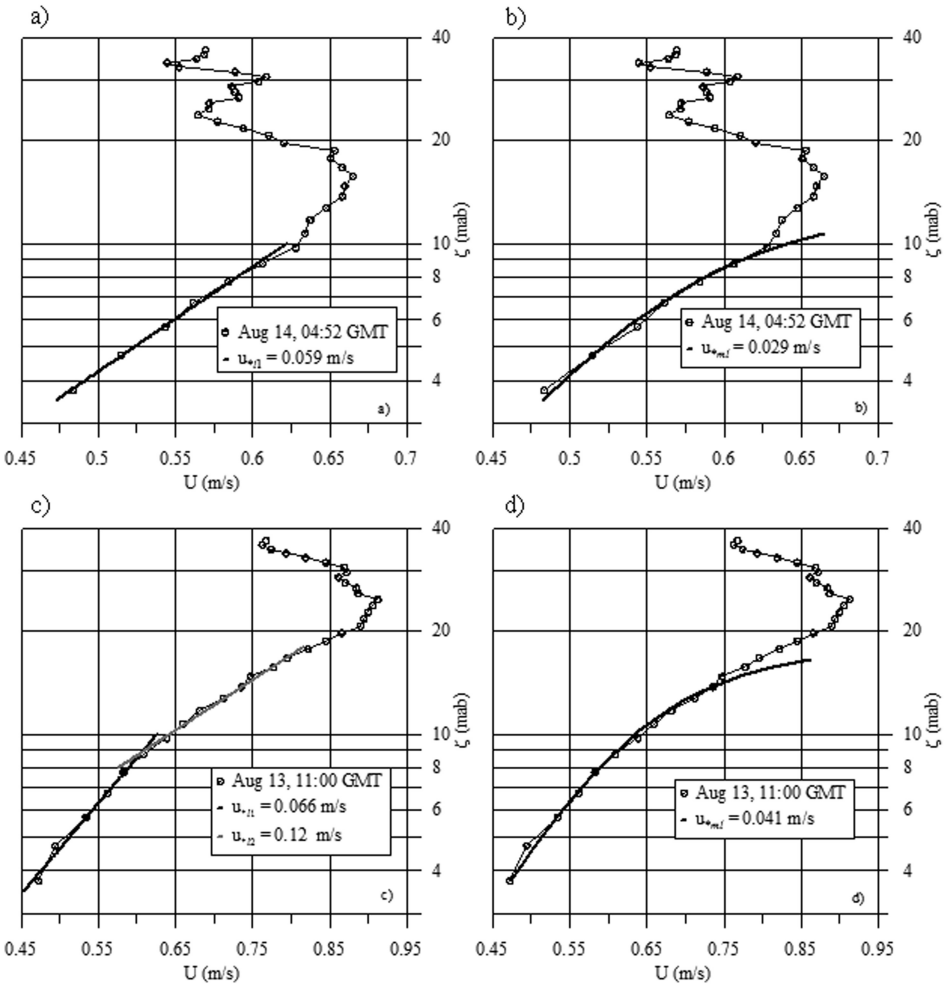

Figure 4. Examples of the velocity profiles with single (a) and double (c) logarithmic segments comparing with corresponding MLL (equation 5) approximations (b) and (d) for the same profiles.

tidal flows varied between 3–5 and 10–15 m, being ∼10 m on average with the root mean square (rms) deviation rms(h_{l1}) = 2.6 m in the present case (see Fig. 3).

In geophysical flows, the lower boundary of the log layer in the absence of boundary roughness is $\sim\nu/u_*$; however, the upper boundary of this wall layer cannot be precisely defined in terms of a single governing parameter, u_*. It has been suggested that the height of the log layer must be much less than $h_f \sim u_*/f$ in nonstratified flows or $h_N \sim u_*/N$ in a stratified flow (e.g., Wimbush and Munk 1970; Zilitinkevich 1972). Pollard, Rhines, and Thompson (1972) proposed that the combined influence of N and f on the boundary layer

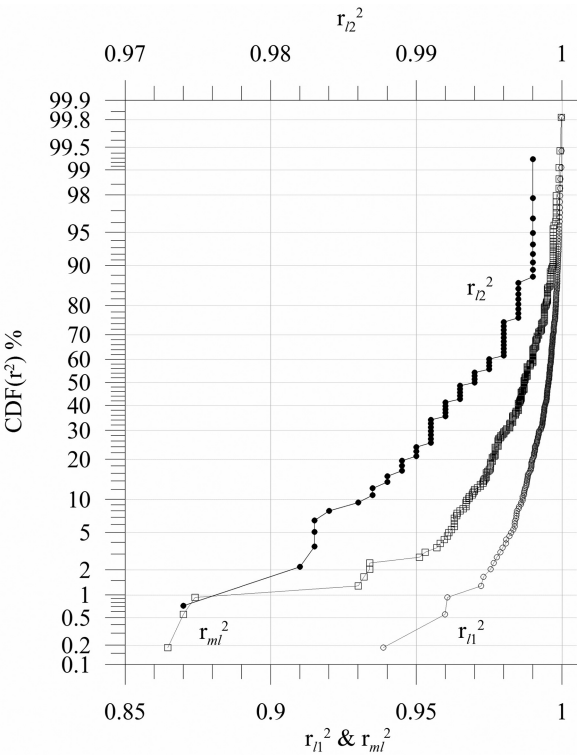

Figure 5. Cumulative distributions of the coefficient of determination for the first (r^2_{l1}, open circles) and second (r^2_{l2}, dots) classic log-layer approximations and for the modified log-layer fits (r^2_{ml}, squares). The upper axis is for r^2_{l2} due to very narrow range of its variability. CDF, cumulative distribution function.

turbulence leads to $h_{Nf} \sim u_*/\sqrt{fN}$, which is a possible estimate for the height of a relatively thick and weakly stratified boundary layer bounded by a sharp density gradient (also see Weatherly and Martin 1978). The scaling factors of proportionality in these formulas vary in a wide range, from 0.5 (Zilitinkevich and Esau 2002) to 1.9 (Lozovatsky et al. 2005). To account for the possible influence of tidal flow on the dynamics of nonstratified rotating BBL, Sakamoto and Akitomo (2008) suggested that the BBL height can be specified as $h_{f\omega} \sim u_*/|f + \omega_T|$, where ω_T is the tidal frequency (positive when the tidal ellipse is cyclonic). In the spirit of Pollard, Rhines, and Thompson (1972), one may specify the tidal BBL height with overlying stratification as $h_{Nf\omega} = c_{Nf\omega}u_*/\sqrt{N|f + \omega_T|}$ with the factor $c_{Nf\omega}$ close to unity. Additional formulations for the heights of the stratified boundary layers are also available (e.g., Dallman, Di Sabatino, and Fernando 2013). In all, the friction velocity is an imperative for analysis of various properties of BBL dynamics, and thus accurate estimation of it warrants careful study.

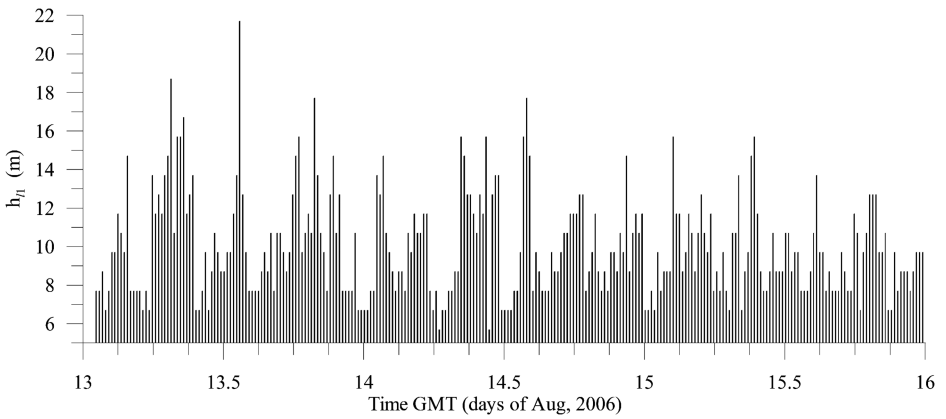

Figure 6. The height h_{l1} of the lower (classic) logarithmic layer during 70 h of observations.

ii. The estimates of friction velocity. The approximation (equation 1) for U (ζ) has been a traditional method of estimating the friction velocity $u_* \equiv u_{*l}$ near the seafloor in the absence of direct measurements of momentum flux components $\overline{u'w'}$ and $\overline{v'w'}$. The accuracy of this method depends on the wellness of the log fit and flow satisfying the basic assumptions that underlie equation (1). As mentioned, the lower segments of all 270 U (ζ) profiles could be fitted by equation (1) with low statistical uncertainty (Fig. 5) for u_{*l1} (subscripts 1 and 2 refer to lower and upper log layers, respectively). The estimates of u_{*l1} (which ranged from 1.8×10^{-2} to 8.8×10^{-2} m s^{-1}), aerodynamic roughness ζ_0, and the mean velocity U_{hl1} at the upper boundary h_{l1} of the logarithmic layer are shown in Figure 7 along with the tidally induced sea surface elevation ξ, with all three showing semidiurnal and quarter-diurnal tidal variability. The semidiurnal minima of u_{*l1} and ζ_0 always preceded the high tide. The following quarter-diurnal minima of running-averaged $\tilde{u}_{*l1}$ and $\tilde{\zeta}_0$ that preceded the low tide are less pronounced, specifically for $\tilde{u}_{*l1}$. The low-frequency variation of u_{*l1} is in good correlation with ζ_0, in that the increase/decrease of u_{*l1} is generally in phase with ζ_0. It is expected as ζ_0 is an adjusted parameter of the log fitting, not a direct representation of the physical roughness of the seabed. The estimate averaged during six semidiurnal cycles of such obtained friction velocity $< u_{*l} >= 5.6 \times 10^{-2}$ m s^{-1}, which are higher than most previously reported values. For instance, a characteristic value of $u_{*l} \approx (1\text{–}7) \times 10^{-3}$ m s^{-1} was obtained by Lozovatsky et al. (2012) based on the log-layer approximation of U (ζ) for the lower 0.5 m of the water column on the inner shelf of the ECS. Matsuno et al. (2005) reported relatively small $u_* = 4 \times 10^{-3}$ m s^{-1} near the ECS shelf break. Much higher values of $u_* = 2 \times 10^{-2}$ m s^{-1} were found in Pickering Passage (Sternberg 1968), $u_* = (1\text{–}4) \times 10^{-2}$ in Puget Sound (Gross and Nowell 1983), and $u_* = 1.1 \times 10^{-2}$ m s^{-1} on the Virginia shelf (Kim et al. 2000) to name a few studies. A good correspondence between the log-layer u_{*l} and skin-layer u_{*s} (acoustic Doppler velocimeter [ADV] measurements at $\zeta = 0.9$ mab) was reported by Lozovatsky et al. (2008b) for reversing tidal currents on

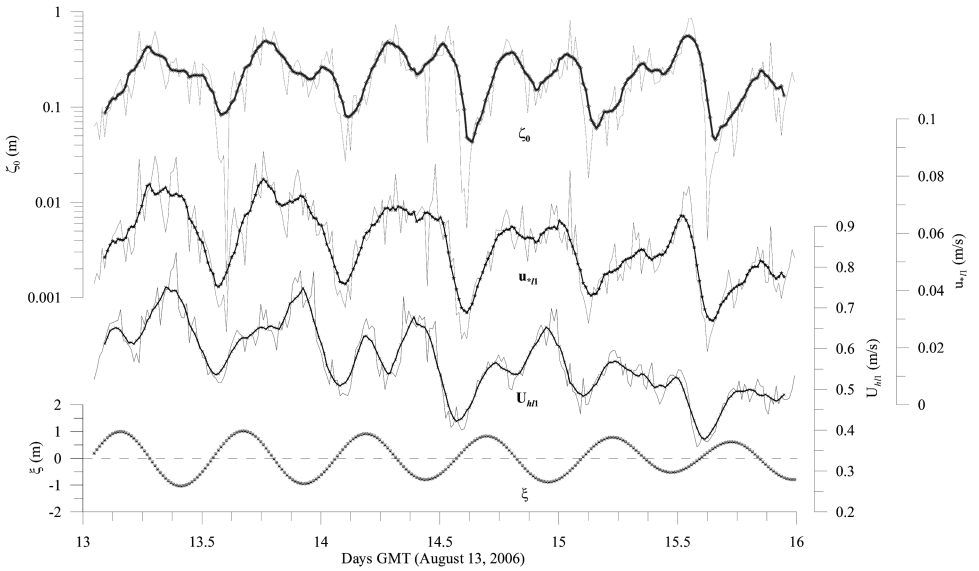

Figure 7. Friction velocity u_{*l1}, aerodynamic roughness ζ_0, velocity amplitude U_{hl1} at the upper boundary of the lower logarithmic layer, and the barotropic elevation of the sea surface ξ (the time step $\Delta t = 16$ min); the nine-point running-averaged data are shown by different symbols.

a shallow ECS shelf. They also found that u_{*l} in the thick BBL (>10 m height) in the deeper regions of ECS affected by the rotating tidal flow is approximately twice that of u_{*s}. Unusually high values of u_{*l} obtained in our study suggest that u_{*l1} shown in Figure 7 could have been substantially overestimated due to the fact that seemingly logarithmic sections of the observed velocity profiles are also influenced by factors other than classical wall-layer dynamics.

Howarth and Souza (2005) hypothesized that large turbulent eddies (approximately several meters) of the outer region may be responsible for larger values of a log-layer-based u_{*l} compared with the near-bottom ADV measurements of u_{*s} that are relatively unaffected by large eddies. This reflects the possibility of several characteristic scales in the flow that may affect log-layer structure (Long and Chern 1981). Grant and Madsen (1986) stated that the log or log-deficit velocity profiles in topographically affected or stratified or non-stationary oscillatory flows should depend on the length scales pertaining to the governing processes of such flows, in addition to scales relevant to the bottom roughness. In the BBL extended 10 m and more from the seafloor, the boundary layer thickness (properly defined, for example $\sim u_*/N$, if the layer is stratified) became an important scale in the upper part of the BBL. The part of a boundary layer velocity profile may still look logarithmic, but the fit (equation 1) returns estimates of u_* and ζ_0 that are only proportional to the real values, with the former being larger. It has already been argued that the form drag induced by sand

ripples and small-scale bathymetric features can produce a larger u_{*l} compared with the skin-layer u_{*s} (see Smith and McLean 1977; Chriss and Caldwell 1982; Dewey and Crawford 1988; Friedrichs and Wright 1997; Lueck and Lu 1997; Foster, Beach, and Holman 2000; Kim et al. 2000). This effect, added to the pure bottom stress, may lead not only to an artificial increase of u_{*l} but also to a secondary log layer (Sanford and Lien 1999) that will be examined next. The potential influence of stratification in the BBL on the estimates of u_{*l} is explored in Section 3d.

b. Double log-layer structure

The possibility of a double log-layer structure of U (ζ) profiles has been discussed by Sanford and Lien (1999), who attributed it to the increase of momentum flux with ζ in the upper log layer, while stress in the bottom log layer remained constant with ζ. The estimates of friction velocity u_{*l2} in the upper log layer based on equation (1) appeared to be larger than that in the lower layer u_{*l1} by a factor of 1.8, on average. The authors speculated that the form drag produced by upstream seabed morphology could cause the overestimation of u_{*l2} (see also Chriss and Caldwell 1982; Dewey and Crawford 1988; Li 1994; Lueck and Lu 1997).

The concept of multiple logarithmic layers was applied to those profiles with two consecutive logarithmic segments (see example in Fig. 4c). The thickness of the upper logarithmic layer ranged from 3 to 13 m, the mean $< H_{l2} >= 6.9$ m, and rms(H_{l2}) = 1.9 m, with the upper boundary extending to ζ = 11–21 mab. Note that the data obtained by Sanford and Lien (1999) in Pickering Passage showed the lower log layer up to $\zeta = 3$ mab and the upper log layer between $\zeta = 5$ and $\zeta = 12$ mab. Our current measurements in the ECS are all above $\zeta = 3.7$ mab; therefore, it is possible that the observed lower log layer (starting from 3.7 mab) is more similar to the upper log layer of Sanford and Lien (1999), affected by form drag and/or stratification. Thus, the classic logarithmic layer (equation 1) between $\zeta \approx 0$ and $\zeta = 3.7$ mab could have been missed. If so, the upper log layer, conceivably observed in 69 of the ECS profiles in the range of (5.7–10.7) $< \zeta <$ (10.7–20.7) mab, may be indicative of the triple logarithmic layer structure of U (ζ).

The values of u_{*l2}, based on fitting equation (1) to the upper log segments, varied between 5.8×10^{-2} m s^{-1} and 14.3×10^{-2} m s^{-1} with a mean $\langle u_{*l2} \rangle = 9.8 \times 10^{-2}$ m s^{-1}. It is interesting that the ratio $\langle u_{*l2} \rangle / \langle u_{*l1} \rangle = 1.65$ in our case is roughly the same as that of Sanford and Lien (1999), $\langle u_{*l2} \rangle / \langle u_{*l1} \rangle = 0.043/0.024 = 1.79$. Variation of $u_{*l2}\,(t)$ is shown in Figure 8, along with the amplitude of barotropic tide $U_{BT}\,(t)$ and $u_{*l1}\,(t)$ that are given for reference. The upper log layer in Figure 8 generally coincides with local maxima of the bin-averaged $\tilde{u}_{*l1}$. The upper log layer was predominantly observed during the short transition phase of decreasing U_{BT}, approaching its minimum in each quarter-diurnal cycle. The internal wave episodes reported in Lee et al. (2006) were mostly observed in the same tidal phase, and hence, there is a possibility that these phenomena are interrelated. The momentum flux associated with internal waves near the upper boundary of BBL, $h_{BL} \sim h_{l2}$,

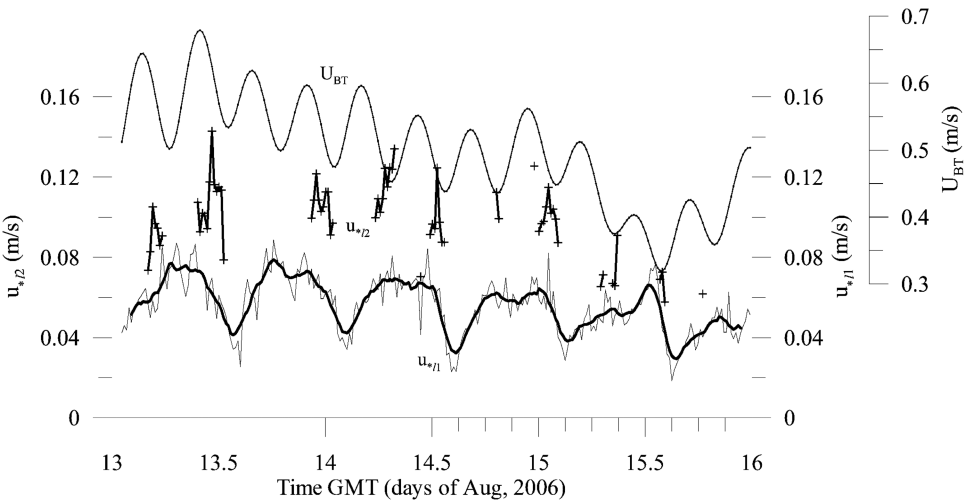

Figure 8. The estimates of u_{*l2} in the upper log layer (69 black crosses) in the background of barotropic tidal velocity U_{BT} (line with symbols). The lower log-layer friction velocity is in light gray along with the nine-point running averaged approximation (bold line).

could have affected the boundary-generated fluxes, thus producing the upper logarithmic layer below h_{l2}. In such cases, u_{*l2} cannot be representative of the friction velocity u_{*s} near the seafloor.

Although the regression of u_{*l2} on u_{*l1} demonstrated approximately a linear trend, the scatter was pretty high ($r^2 = 0.45$), which could be attributed to such sources as the form drag or internal wave–induced momentum flux, which presumably generates the upper log layer but also intermittently affects the lower log layer. This effect may "contaminate" a genuine log-layer friction velocity, $u_{*l} \equiv u_{*s}$, inflating its values to the observed u_{*l1}. Because small-scale bathymetric features in the region are unknown, it is not possible to elaborate on the form-drag hypothesis further.

c. *Log-wake approximation*

The majority of observed ADCP profiles appear to have a distinct velocity maximum just above the upper boundary of the log-layer structure (see Figs. 4 and 9). Similar velocity structure has been observed in the ECS (Lozovatsky et al. 2008a) and modeled as a sum of the log layer (equation 1) and an oscillatory tidal flow (with constant eddy viscosity) at its upper boundary This model, however, does not change u_{*l1} deduced from the classic log-layer approximation (equation 1). Subsequently, we explore the applicability of the model proposed by Coles (1956),

$$\frac{U(\zeta)}{u_*} = \left(\frac{1}{\kappa}\ln\frac{\zeta u_*}{\nu} + B\right) + \frac{2\Pi}{\kappa}\sin^2\frac{\pi\xi}{2}, \tag{2a}$$

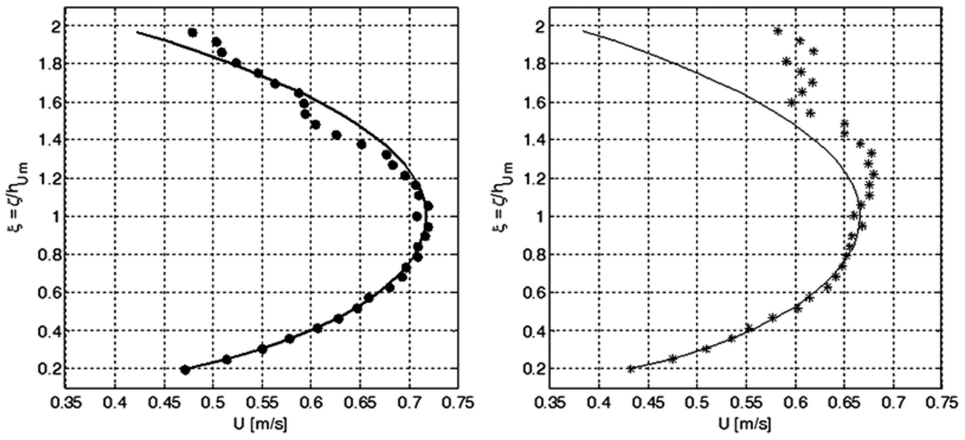

Figure 9. Examples of the velocity profiles measured on (a) 13 August, 17:55, and (b) 14 August, 5:25, fitted by the wake-log-layer law (equation 2b).

where $\xi = \zeta / h_{BL}$ and h_{BL} is the height of the BBL. The first term on the right side of equation (2a) is the logarithmic law with an additive constant B; the second term is the "law of the wake" (Coles 1956; Hinze 1975, p. 698), which accounts for the deviation from the log layer away from the boundary; and Π is Coles' wake strength, accounting for the effect of the Reynolds number. Formula (2a) was later modified by Guo and Julien (2003) and Guo, Julien, and Meroney (2005) for a zero-pressure gradient channel flow as follows:

$$\frac{U(\zeta)}{u_*} = \left(\frac{1}{\kappa}\ln\frac{\zeta u_*}{\nu} + B\right) + \frac{2\Pi}{\kappa}\sin^2\frac{\pi\xi}{2} + \frac{\xi^3}{3\kappa}. \tag{2b}$$

The sine-square term in the law of the wake expresses the effects of the convective inertia in zero-pressure gradient boundary layers and the cubic function forces the log law gradient to be zero at the maximum velocity (Guo and Julien 2008).

Although equation (2b) may arguably be appropriate for reversing tidal flows in estuaries and straits, its applicability to rotating tidal flows away from the coasts is still questionable. In the ensuing analysis, we used Guo and Julien's (2003) approach of calculating the height h_{Um} of the velocity maximum U_M at the upper boundary of the BBL by fitting a parabola $u = a\xi^2 + b\xi + c$ near the point of maximum velocity (for $\xi = \frac{\zeta}{h_{Um}} > 0.6$), which gives $h_{Um} = -b/2a$. Figure 9 shows examples of velocity profiles approximated by equation (2b). When the flow above the BLL is not disturbed by small-scale process (e.g., internal waves) formula (2b) is perfectly fitted to the data (see Fig. 9a); however, more often the fit is good only over the logarithmic section Significant deviations can be seen thereafter (Fig. 9b). The corresponding friction velocities $u_* \equiv u_{*lw}$ and adjustable parameters B

and Π were estimated using the MATLAB curve-fitting tool that minimizes fitting errors. In some cases, the data showed good agreement with the log-wake model (equation 2b), occurring within and above the log layer. The estimates of friction velocities, however, did not change much from u_{*l1}. It was found that $\langle u_{*lw} \rangle = 0.94 \langle u_{*l1} \rangle$, suggesting that simple nonstratified unidirectional flow models of BBL dynamics may not provide a robust methodology for estimating boundary shear stress, $\tau_s = u_{*s}^2$, in the ECS. An MLL model (Perlin et al. 2005) that accounts for stable stratification in the BBL is thus explored next.

d. MLL model: Influence of stratification

i. Velocity profiles. The application of equation (1) to a noncompletely homogeneous ocean BBL, which often contains weak remnant stratification, leads to an overestimation of the friction velocity u_{*l} compared with the skin-layer friction velocity u_{*s}. The disparity, in general, has been attributed to various processes that may affect the log and log-deficit flow profiles by imposing additional scales (Grant and Madsen 1986). As has been mentioned, these could be the form drag (Sanford and Lien 1999), rotation of the flow vector (Lozovatsky et al. 2008b; Yoshikawa et al. 2010), and stratification (Perlin et al. 2005). Subsequently, a slightly modified model of Perlin et al. (2005) is used to assess the effect of stratification on friction velocity estimates deduced from the ADCP profiles in the ECS.

The novelty of this model is the formula for integral turbulent length scale,

$$l_{BL} = l_c \left(1 - \frac{\zeta}{h_d}\right), \tag{3}$$

which combines the classic boundary layer scale $l_c = \kappa\zeta$ for nonstratified flows with the buoyancy (or the Dougherty-Ozmidov) length scale $L_N = \varepsilon^{1/2}/N^{3/2}$ near the upper boundary of the BBL. The latter takes over l_c between h_{l1} and a specific height given by

$$\zeta = h_d = \frac{D}{1 - (L_N/\kappa D)}, \tag{4a}$$

where turbulent eddies generated by the boundary stress are affected by the stable stratification near the upper boundary $\zeta = D$ of weakly stratified BBL (see fig. 2 of Perlin et al. 2005). Note that equation (4a) is based on empirical data obtained over the Oregon shelf (Perlin et al. 2005a). It implies that the turbulent length l_{BL} (equation 3) becomes the Dougherty-Ozmidov scale L_N exactly at $\zeta = D$. Although this sharp transition looks reasonable, it can be relaxed if the boundary is not very sharp, allowing l_{BL} to gradually approach L_N in the vicinity of D (i.e., at $\zeta = c'D$). In this case, equation (4a) is replaced by

$$h'_d = \frac{c'D}{1 - (L_N/\kappa c'D)}. \tag{4b}$$

If $c' > 1$, then $h'_d > D$ and vice versa. Note that with larger c' the buoyancy scale L_N is expected to decrease above D. Using $u_*^2 = K\,(dU/d\zeta)$ for the near-bottom layer, where

eddy diffusivity $K = u_* l_{tr}$ and turbulent scale $l_{tr} = l_{BL}$ (equation 3), with the original formulation (equation 4a) for h_d, the modified velocity profile becomes

$$U(\zeta) = \left(\frac{u_*}{\kappa}\right) \ln\left(\frac{\zeta(h_d - \zeta_0)}{\zeta_0(h_d - \zeta)}\right). \tag{5}$$

This model was employed to calculate the friction velocity $u_* \equiv u_{*ml}$ by fitting all 270 ADCP profiles to equation (5) using the MATLAB curve-fitting capability. The height h_d was treated as an adjustable parameter to achieve the best fit, in terms of the coefficients of determination r^2 that are shown in Figures 5 and 10 for all $U(\zeta)$ profiles. The upper boundary of the MLL fitting h_{ub} was picked visually as the location where equation (5) starts permanently departing from data lowering r^2 (see examples in Fig. 4b and d). It appears that the MLL model could be successfully used to approximate the single as well as double log-layer profiles (Fig. 4b and d). It also provides substantially lower values of friction velocity compared with the classical log-layer model.

ii. MLL friction velocity. In Figure 10, the friction velocity $u_{*ml}(t)$ evaluated using equation (5) is compared with $u_{*l1}(t)$ deduced from equation (1); the corresponding coefficients of determination $r^2(t)$ are also shown. The time variation of $r^2_{ml}(t)$ appears to be more dispersed than that of $r^2_{l1}(t)$, likely because the MLL fittings encompass longer segments of the velocity profiles, which are governed not only by the bottom stress but also by the stratification, following equation (5). Segments with the lowest estimates of friction velocity coincide with the lowest values of r^2_{ml}, which may indicate a higher influence of nonboundary dependent processes in shaping low-amplitude velocity profiles in the BBL. It is interesting that the minimal r^2_{ml} (down to ~0.87, in the first three cases between $t = 13.6$ and $t = 14.7$; Fig. 10) coincided with the flow essentially directed to the west, generally from deeper to shallower depths. The ADCP temperature sensor registered a decrease of the near-bottom temperature of ~0.2°C–0.3°C during this phase of rotating tidal flow, leading to an increase of the temperature gradient (density stratification) in the lower BBL; these conditions do not reflect the tenets of the MLL formulations (3) and (4a).

The upper boundary of the MLL $h_{ub}(t)$ and the transition height $h_d(t)$ in Figure 10 are well correlated with quarter-diurnal tidal harmonics and higher-frequency oscillations. The difference between the means, $\Delta h = \langle h_d \rangle - \langle h_{ub} \rangle = 13.8 - 10.4 = 3.4$ m, is similar to that obtained by Perlin et al. (2005b) at the Oregon shelf. Figure 10 also shows that both estimates of the friction velocity are subjected to the same main variations as the mean velocity $U_{ub}(t)$ at $\zeta = h_{ub}$. The quarter-diurnal periodicity is more pronounced in $u_{*ml}(t)$ compared with $u_{*l1}(t)$, and the amplitude of $u_{*ml}(t)$ semidiurnal component is smaller than that of $u_{*l1}(t)$. The difference is especially evident during the phases of low $U_{ub}(t)$, whence minima of $u_{*l1}(t)$ are much deeper than those of $u_{*ml}(t)$. The observations suggest that the absolute values of $u_{*ml}(t)$ are approximately half of $u_{*l1}(t)$; namely, the averaged $\langle u_{*ml} \rangle = 2.9 \times 10^{-2}$ m s^{-1} whereas $\langle u_{*l1} \rangle = 5.3 \times 10^{-2}$ m s^{-1}, and the upper log-layer u_{*l2} appears to be a factor of 2.6 larger than u_{*ml}.

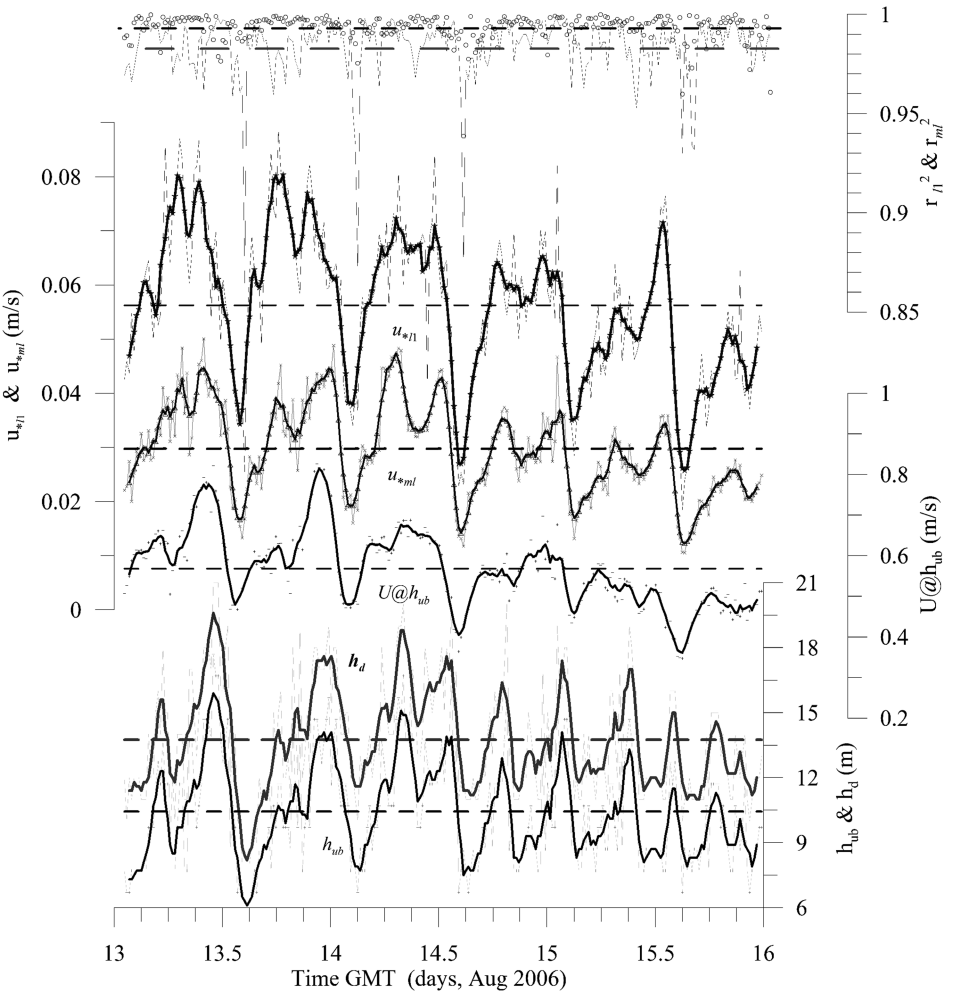

Figure 10. Time series of the friction velocity in the classical logarithmic layer u_{*l1} and in the modified log layer (MLL) u_{*ml} compared with the velocity magnitude at the upper boundary of MLL $U@h_{ub}$. The confidence of determination r^2 for classic (small circles) and MLL (thin gray line) approximations are on the top. The mean values of all variables for the period of observations are shown by dashed lines; h_{ub} and h_d are specified in the text. Bold lines are five-point running averages.

The calculation of drag coefficient, $C_{Dm} = u_{*mll}^2/U_A^2$, where U_A is the amplitude of the suitably defined mean velocity, is not straightforward in non-well-mixed rotating BBL flows. In previous studies, a characteristic mean velocity, U_A, has been specified at various heights above the seafloor, including (1) at the lowest level of measurements (Lozovatsky

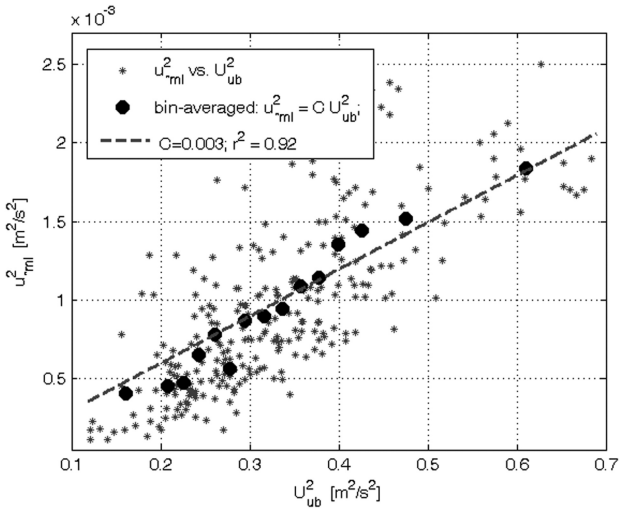

Figure 11. The squared modified log-layer (MLL) friction velocity versus the squared mean velocity magnitude at the upper boundary of the MLL (small stars) and the bin-averaged estimates of the same variables (18 samples per bin) approximated by the linear trend (dashed line) shown in the legend.

et al. 2008b, 2012); (2) a "standard," $\zeta_A = 1$ mab (e.g., Ludwick 1975; Bowden 1978; Elliott 2002); or (3) a specific arbitrary level (e.g., 5 mab or even 20 mab; Perlin et al. 2005), based on the availability of data.

When the squared MLL friction velocity u^2_{*ml} is regressed with the squared flow amplitude $U^2_A \equiv U^2_{3.7\text{mab}}$ at the first level of ADCP data $\zeta_1 = 3.7$ mab, which is somewhat away from the seafloor, no meaningful correlation was found. The same was true for the correlation between u^2_{*ml} and the squared barotropic tidal velocity $U^2_A \equiv U^2_{BT}$. However, when u^2_{*ml} was plotted against the squared magnitude of the mean velocity $U^2_A \equiv U^2_{ub}$ at the upper boundary of the MLL h_{ub} (Fig. 11), a linear regression, $u^2_{*ml} = CU^2_{ub}$ with $C = 3 \times 10^{-3}$, was found, with 95% confidence bounds (2.85–3.13) $\times 10^{-3}$. The value of $C = 3 \times 10^{-3}$ is close to the commonly quoted $C_d = 2.5 \times 10^{-3}$, but whether it is relevant to the traditional drag concept remains unclear. The correlation between u^2_{*ml} and U^2_{ub} is relatively low ($r^2 = 0.54$), indicating that the u_{*ml} estimates are influenced not only by the tidal flow but also by other dynamic processes near the upper boundary of the BBL where stratification affects the vertical distribution of momentum flux. Other factors, such as internal wave–generated momentum flux, horizontal inhomogeneity, and unsteadiness of the flow may also play role.

e. The height of BBL and MLL

To gain further insights into BBL dynamics, several TurboMAP profiles obtained between 20:30 and 22:00 GMT on 13 August from a drifting ship ~2 km to the north from the

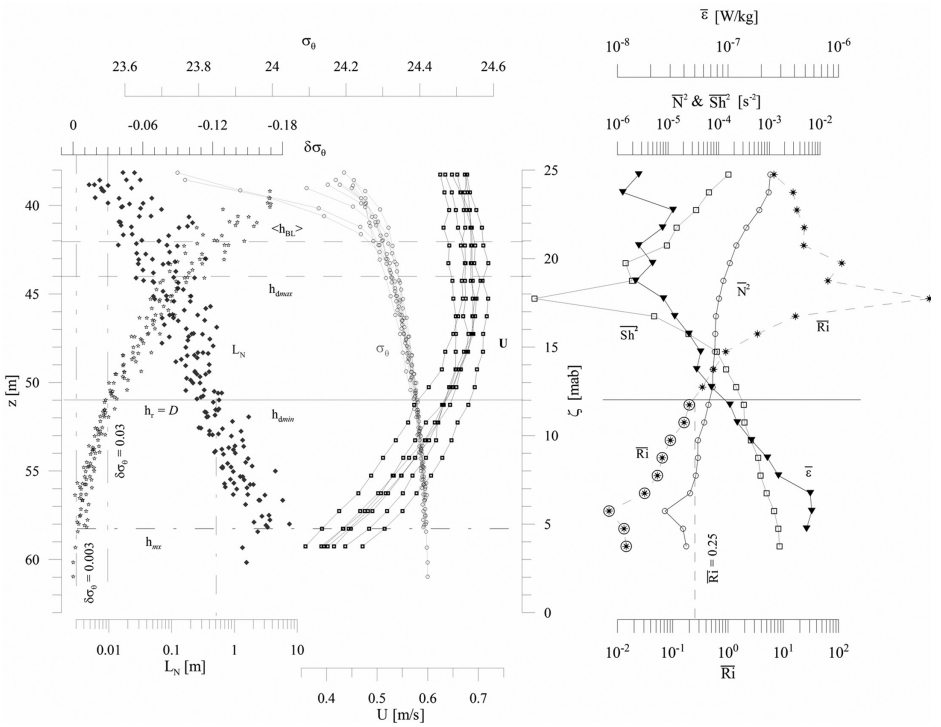

Figure 12. Left: Profiles of the potential density anomaly $\sigma_\theta(z)$, circles; measure of homogeneity $\delta\sigma_\theta(\zeta)$, stars; Dougherty-Ozmidov scale $L_N(\zeta)$, gray diamonds; and velocity amplitude $U(\zeta)$, squares, during 1.5 h of the R/V *EARDO* drift near the acoustic Doppler current profiler mooring. Right: Time-averaged profiles of the squared shear $\overline{Sh^2}$, buoyancy frequency $\overline{N^2}$, Richardson number $\overline{Ri}$, and dissipation rate $\bar{\varepsilon}$ corresponding to the data shown in the left panel.

ADCP mooring were analyzed. Figure 12 (left panel) shows six ADCP velocity profiles, $U(\zeta)$,along with nine profiles of the potential density anomaly $\sigma_\theta(z)$, the Dougherty-Ozmidov buoyancy scale $L_N(z)$, and a measure of homogeneity, $\delta\sigma_\theta(\zeta) = \sigma_\theta(\zeta) - \sigma_\theta(\zeta_{\text{end}})$, where $\sigma_\theta(\zeta_{\text{end}})$ is the density obtained at the end point ζ_{end} closest to the seafloor. According to Perlin et al. (2005), the height of bottom mixed layer h_{mx} is defined as the maximum distance from the seafloor, where $\delta\sigma_\theta(\zeta = h_{mx}) \leq 0.6 \times 10^{-3}$. The height of the so-called remnant mixed layer h_r, which is above h_{mx}, is the distance from the bottom where $\delta\sigma_\theta(h_r) = \delta\sigma_\theta(\zeta) \leq 3 \times 10^{-2}$. The end point of our σ_θ profiles is quite far from the seafloor ($\zeta_{\text{end}} \approx 2$ mab for only one profile), but it is possible to detect the height of the well-mixed near-bottom layer h_{mx} at the crossing of the vertical triple-dotted dash line, $\delta\sigma_\theta(\zeta < h_{mx}) = 3 \times 10^{-3}$, and the horizontal single-dotted dash line, $h_{mx} = 4$–5 mab (Fig. 12). The mixed-layer height h_{mx} is approximately the same as that reported by Perlin et al. (2005), although $\delta\sigma_\theta(\zeta)$ in our case is five times less restrictive than that of Perlin, Moum,

and Klymak (2005) and Perlin et al. (2007). The height of the remnant layer h_r is quite easy to identify in Figure 12 using the original (Perlin, Moum, and Klymak 2005) criterion for h_r, which leads to $h_r = 11$–12 mab (the crossing between the vertical double-dotted dash line and the horizontal straight line). Perlin et al. (2007) reported $L_N\,(\zeta = D) \approx 0.4$ m, which is well correlated with $L_N\,(\zeta \approx h_r)$ shown by the vertical single-dotted dash line in Figure 12. Thus, the estimates of h_r can be treated as those of D in formulas (4a) and (4b). As mentioned in Section 3d(i), h_d specified by equation (4a) should lie somewhere above D, but the approximation (equation 5) does not require strict following of equation (4a), allowing it to be replaced by equation (4b) with an arbitrary constant, $c' \sim \mathrm{O}(1)$. The adjustable h_d was found to be in the range from $h_{d\,\min} = 12$ to $h_{d\,\max} = 19$ for the $U(\zeta)$ profiles shown in Figure 12. This means that $h_{d\,\min}$ is coincident with $h_r = D$, leading to $c' = 1$ and $h_{d\,\max}$ requiring $c' \approx 1.6$.

The remnant mixed layer in the ECS BBL was not capped by a sharp pycnocline but overlaid by a weakly stratified layer that extended up to the lower boundary of the main pycnocline h_{BL} at $z = 42$–44 m (the correspondent $\zeta \equiv h_{BL} = 19$–21 mab marked in Fig. 12 by long-dashed horizontal lines). The stratification at h_{BL} is an order of magnitude weaker than that in the pycnocline, but it is still relatively high, $N^2 \sim (1\text{–}2) \times 10^{-4}\mathrm{s}^{-2}$, gradually decreasing to $\sim 2 \times 10^{-5}\ \mathrm{s}^{-2}$ at h_{mx}. The buoyancy scale is very small above $h_{BL}(L_N = 1$–10 cm), increasing to $L_N = 3$–4 m closer to the seafloor. The h_{BL} is mostly governed by the balance between the boundary stress, inertial forces in the BBL, buoyancy in the pycnocline, and tidal forcing, namely, $h_{BL} \sim h_{Nf\omega} = c_{Nf\omega} u_* / \sqrt{N\,|f + \omega_T|}$, which is inferred in Section 3a(i) as a modified formulation of Sakamoto and Akitomo (2008). For semidiurnal clockwise rotating tide, the mean $\hat{u}_{*ml} = 2.9 \times 10^{-2}\ \mathrm{m\ s}^{-1}$, and characteristic pycnocline $\hat{N}^2 \approx 5 \times 10^{-4}\ \mathrm{s}^{-2}$, the $h_{Nf\omega}$ appears to be a good estimate of h_{BL}, providing $c_{Nf\omega} \approx 0.8$.

f. Turbulence in the BBL

The TurboMAP measurements from the drifting ship during 1.5 h allowed comparison of the averaged profiles of the kinetic energy dissipation rate $\bar{\varepsilon}\,(z)$ with the ADCP-based averaged profile of squared vertical shear $\overline{Sh^2}\,(\zeta)$, the TurboMAP-based profile of the squared buoyancy frequency $\overline{N^2}\,(z)$, and thus the gradient Richardson number profile $\overline{Ri}\,(\zeta) = \overline{Sh^2}/\overline{N^2}$. Nine TurboMAP and six ADCP individual profiles were used for averaging; the height from the bottom and the depth z are related as $\zeta = 63 - z$. The TurboMAP averaged profiles were interpolated to the times and levels of the ADCP profiles; the result is shown in the right panel of Figure 12. The dissipation rate in the BBL $\bar{\varepsilon}\,(z)$ generally increases downward from $\sim 10^{-8}\ \mathrm{W\ kg}^{-1}$ at $\zeta = 25$ mab to $\sim 10^{-6}\ \mathrm{W\ kg}^{-1}$ at the end of the casts, which is $\zeta = 4$–5 mab. The buoyancy frequency rapidly decreases toward the seafloor from $\overline{N^2} \sim 10^{-3}\ \mathrm{s}^{-2}$ at $\zeta = 25$ mab to $\overline{N^2} \sim 10^{-5}\ \mathrm{s}^{-2}$ at $\zeta = 4$–5 mab. The shear profile exhibits a distinctive minimum near $\zeta = h_{d\,\max} = 19$ mab, associated with the maxima of $U\,(\zeta)$ at this height, which led to very high values of $\overline{Ri}$. Below the maximum, $\overline{Ri}$ rapidly

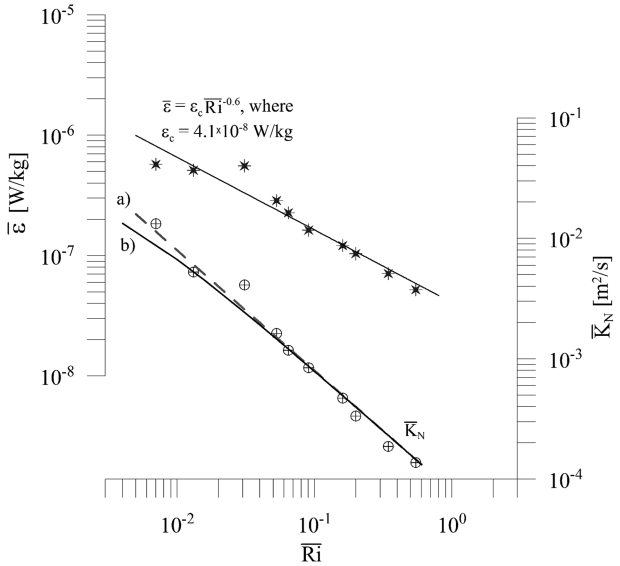

Figure 13. Averaged dissipation rate $\bar{\varepsilon}$ and the diffusivity $\bar{K}_N$ in the bottom boundary layer between $\zeta = 4$ and 14 mab as functions of the Richardson number $\overline{Ri}$. The approximations a) and b) follow equations (7a) and (7b), respectively.

decreases, becoming less than 0.25 at $\zeta < 12$ mab. Thus, turbulence in the lower BBL can be generated not only by the bottom stress but also by local shear instabilities, which may enhance the momentum flux (friction velocity). It appears that the averaged dissipation rate below $\zeta = 12$–14 mab can be approximated by a power law,

$$\bar{\varepsilon} = \varepsilon_c \overline{Ri}^{-0.6}, \text{ where } \varepsilon_c = 4.1 \times 10^{-8} \text{ W kg}^{-1} \tag{6}$$

(Fig. 13), with $r^2 = 0.93$. Due to the small number of data points (only 10) and a short segment (1.5 h) of the tidal cycle employed, the obtained parameters of equation (6) are not expected to be universal. When the diffusivity $\bar{K}_N = \gamma \bar{\varepsilon} / \overline{N^2}$ (calculated with traditional constant mixing efficiency $\gamma = 0.2$) was regressed on $\overline{Ri}$ (Fig. 13), the dependence $\bar{K}_N \left(\overline{Ri}\right)$ appeared to be strong:

$$\bar{K}_N = K_c \overline{Ri}^{-1}, \tag{7a}$$

with $r^2 = 0.97$ and $K_c = 8 \times 10^{-5}$ m^2 s^{-1}. The factors ε_c and K_c are characteristic values of the corresponding variables when $\overline{Ri}$ is slightly above $Ri_c = 0.25$. Note that the empirical approximation (equation 7a) can be rewritten in a more general form (Lozovatsky et al. 2006), in the spirit of Munk and Anderson (1948):

$$\bar{K}_N = \frac{K_0}{\left(1 + \overline{Ri}/Ri_c\right)^p}, \tag{7b}$$

where for this case $p = 1$, the diffusivity in a nonstratified flow $K_0 = 4 \times 10^{-2}$ m^2 s^{-1}, and $Ri_c = 0.002$. In the boundary layer near the seafloor (for $\zeta < \zeta_0$), K_0 can be introduced as

$$K_0 = u_* \kappa \zeta. \tag{7c}$$

At the distances $\zeta > \zeta_0$, the stratification starts to a play role making $\overline{Ri}$ positive. It is reasonable to assume that $\zeta_0 < 3$–4 mab because our data are taken above this level and are already affected by stratification. Using the averaged MLL friction velocity obtained for this data segment, $u_* \equiv \langle u_{*ml} \rangle_{1.5\mathrm{h}} = 3.6 \times 10^{-2}$ m s^{-1} and $\kappa = 0.4$, $K_0 = 4 \times 10^{-2}$ m^2 s^{-1} corresponds to $\zeta = \zeta_0 = 2.8$ mab, which is a very reasonable estimate of ζ_0. Thus, the closeness of the independent estimates of K_0 based on the profiling measurements of the dissipation rate and buoyancy frequency (equation 7b) and the MLL friction velocity (equation 7c) suggest that the application of the MLL model (equation 5) to ADCP velocity profiles in a weakly stratified BBL leads to reasonable friction velocities, u_{*ml}, that may well represent the skin-layer friction velocity in the BBL of the ECS.

4. Summary

The BBL dynamics of the ECS were studied using a 70 h long ADCP-600 kHz bottom mooring, which provided 270 sixteen-minute bin-averaged velocity profiles, $U(\zeta, t)$, where ζ is a distance from the seafloor and t is the time. The tidal-cycle averaged water depth of the measurement location was 63 m. The amplitude of the clockwise rotating barotropic tidal vector decreased from 0.68 m s^{-1} to 0.32 m s^{-1}, and the amplitudes of surface elevation ξ_{BT} reduced from ~1 to 0.7 m.

All 1 m sampled $U(\zeta)$ profiles contained segments of different lengths that could be fitted well to the classical log-layer formula (equation 1), starting from the first ADCP bin ($\zeta = 3.7$ mab). Of the 270 profiles, 69 exhibited a second log-layer segment. The mean height of the upper boundary of the first (lower) logarithmic layer was $<h_{l1}> = 10$ mab, with an rms$(h_{l1}) = 2.6$ m. The upper logarithmic layer occupied the depth range of ζ between 5.7–10.7 and 10.7–20.7 mab; the mean thickness $\langle h_{l2} \rangle = 6.9$ m, and the rms$(h_{l2}) = 1.9$ m. On average, the classical log-layer estimate of the friction velocity u_{*l1} was ~1.65 times smaller than u_{*l2}, which is roughly the same ratio (1.79) as that reported by Sanford and Lien (1999). It is possible that the momentum flux carried by internal waves near the BBL upper boundary, $h_{BL} \approx h_{l2}$, could affect the bottom boundary-generated flux, producing a seemingly logarithmic layer below h_{l2} with scaling velocity u_{*l2}. In this case, u_{*l2} is not the friction velocity u_{*s} near the seafloor. Nonetheless, the lower log-layer-based u_{*l1} appeared to be unreasonably high, $\langle u_{*l1} \rangle = 5.6 \times 10^{-2}$ m s^{-1}, suggesting that u_{*l1} could be substantially overestimated due to the influence of form drag (Sanford and Lien 1999), stratification (Perlin et al. 2005), and rotation of the tidal vector (Lozovatsky et al. 2008b; Yoshikawa et al. 2010).

The log-wake model (e.g., Coles 1956; Guo, Julien, and Meroney 2005), which accounts for currents above the upper boundary of the logarithmic layer under neutrally stratified

conditions, yielded a very good approximation for the measured $U(\zeta)$ in and above the log layer, but it did not substantially change the estimated friction velocity; on average, $\langle u_{*lw} \rangle = 0.94 \langle u_{*l1} \rangle$. This suggests that simple nonstratified unidirectional flow models do not provide a robust methodology for estimating the boundary stress $\tau_s = u_{*s}^2$ in the ECS.

The MLL model of Perlin et al. (2005) led to substantially (approximately two times) lower scaling velocities, u_{*ml}, compared with the friction velocity u_{*l1} of the lower log layer. The MLL (equation 5) successfully approximated as single as double log-layer velocity profiles. The original MLL approach was extended to allow the BBL turbulent scale (equation 3) to reach the buoyancy scale L_N not precisely at the height of the MLL D as in the original formula (equation 4a) but in the vicinity of $c'D$ (equation 4b), where the factor $1 < c' < 1.6$. This modification accounts for weak stratification in the lower BBL above a remnant mixed layer, instead of a sharp boundary between the BBL and overlaying pycnocline as assumed in equation (4a).

The u_{*ml}-based estimate of $C_{Dm} = u_{*mll}^2 / U_A^2 = (2.8\text{–}3.2) \times 10^{-3}$ was found to be close to the traditional value of drag coefficient, $C_d \approx 2.5 \times 10^{-3}$, notwithstanding that C_{Dm} uses the mean flow U_A at the upper boundary of the modified log layer rather than at a standard height. The previous results indicate that the stratification, specifically near the upper boundary of the BBL, which indirectly influences MLL (through the buoyancy scale L_N), is an important factor of BBL dynamics in the ECS.

A number of TurboMAP profiles were employed to estimate the dissipation rate in the BBL. A thick quasi-homogeneous (weakly stratified) BBL was observed, with its upper boundary at $h_{BL} \sim 19\text{–}21$ m. Aloft the BBL was a sharp thermohalocline rich in fine structure, with $\Delta T \approx 15°\text{C}$ and $\Delta S \approx 4$ psu in the depth range $\sim 40 < z < \sim 15$ m. The height of the BBL, h_{BL}, could be scaled by $h_{Nf\omega} = c_{Nf\omega} u_* / \sqrt{N\,|f + \omega_T|}$, which is a modified formula of Sakamoto and Akitomo (2008) for rotating homogeneous tidal BBL that now accounts for stratification; $c_{Nf\omega}$ was found to be close to 0.8 for our data set.

On average, the dissipation rate in the stratified BBL decreased uniformly upward from the seafloor, with $\varepsilon_{\text{nb}} \approx 2 \times 10^{-6}$ W kg^{-1} at $\zeta = 3.7$ mab, and the observed minimum value was $\varepsilon_{\min} \approx 10^{-9}$ W kg^{-1} near $\zeta = h_{BL}$ The decrease of the dissipation is faster than that predicted by the law of the wall. The empirical data can be approximated by an exponential function, $\varepsilon(\zeta) = \varepsilon_0 e^{-\zeta / L_m}$, where $\varepsilon_0 = 2.8 \times 10^{-6}$ W kg^{-1}, and the scaling length $L_m = 3.3$ m is an integral (mixing) length, which is proportional to the BBL height; the constant of proportionality $c_L = L_m / h_{BL} \approx 0.17$ for the present case.

A high correlation was found between the averaged Richardson number, $\overline{Ri}$, in the lower part of the BBL, where $\overline{Ri}$ decreases below 0.25, and the averaged dissipation rate and the diffusivity $\bar{K}_N = 0.2\bar{\varepsilon} / \overline{N^2}$. The clear inverse dependence of $\bar{K}_N$ on $\overline{Ri}$ (Fig. 13) according to equation (7b) allowed comparing the dissipation/stratification-based empirical estimate of diffusivity of nonstratified flow near to the seabed, K_0, with that derived from the mean MLL friction velocity. The good agreement between the two independent estimates of K_0 indicates the applicability of the MLL model (equation 5) to rotating, tidally driven, weakly stratified BBL in the ECS.

Acknowledgments. The authors are grateful to the scientists and students of the Korean Institute of Ocean Science and Technology and the crew of R/V *EARDO* for arranging the logistics of data collection. The work was partially supported by the U.S. Office of Naval Research (grant N00014-05-1-0245).

REFERENCES

Blackadar, A. K. 1962. The vertical distribution of wind and turbulent exchange in a neutral atmosphere. J. Geophys. Res., *67*(8), 3095–3102.

Bowden, K. F. 1978. Physical problems of the benthic boundary layer. Geophys. Surv., *3*, 255–296.

Burchard, H., P. D. Craig, J. R. Gemmrich, H. van Haren, P.-P. Mathieu, H. E. Markus Meier, W. A. M. Nimmo Smith, et al. 2008. Observational and numerical modeling methods for quantifying coastal ocean turbulence and mixing. Prog. Oceanogr., *76*, 399–442.

Chriss, T. M., and D. R. Caldwell. 1982. Evidence for the influence of form drag on bottom boundary layer flow. J. Geophys. Res.: Oceans, *87*, 4148–4154.

Coles, D. 1956. The law of the wake in the turbulent boundary layer. J. Fluid Mech., *1*(2), 191–226.

Cyr, F., D. Bourgault, and P. S. Galbraith. 2011. Interior versus boundary mixing of a cold intermediate layer. J. Geophys. Res.: Oceans, *116*, C12029. doi: 10.1029/2011JC007359

Cyr, F., D. Bourgault, and P. S. Galbraith. 2015. Behavior and mixing of a cold intermediate layer near a sloping boundary. Ocean Dyn., *65*, 357–374.

Dallman, A., S. Di Sabatino, and H. J. S. Fernando. 2013. Flow and turbulence in an industrial/suburban roughness canopy. Environ. Fluid Mech., *13*(3), 279–307.

Dewey, R. K., and W. R. Crawford. 1988. Bottom stress estimates from vertical dissipation rate profiles on the continental shelf. J. Phys. Oceanogr., *18*(8), 1167–1177.

Egbert, G. D., and S. Y. Erofeeva. 2002. Efficient inverse modeling of barotropic ocean tides. J. Atmos. Oceanic Technol., *19*, 183–204.

Elliott, A. J. 2002. The boundary layer character of tidal currents in the eastern Irish Sea. Estuarine, Coastal Shelf Sci., *55*, 465–480.

Foster, D. L., R. A. Beach, and R. A. Holman. 2000. Field observations of the wave bottom boundary layer. J. Geophys. Res.: Oceans, *105*(C8), 19634–19647.

Friedrichs, C. T., and L. D. Wright. 1997. Sensitivity of bottom stress and bottom roughness estimates to density stratification, Eckernförde Bay, southern Baltic Sea. J. Geophys. Res.: Oceans, *102*(C3), 5721–5732.

Grant, W. D., and O. S. Madsen. 1986. The continental-shelf bottom boundary layer. Annu. Rev. Fluid Mech., *18*, 265–305.

Gross, T. F., and A. R. M. Nowell. 1983. Mean flow and turbulence scaling in a tidal boundary layer. Cont. Shelf Res., *2*(2–3), 109–126.

Guo, J., and P. Y. Julien. 2003. Modified log-wake law for turbulent flow in smooth pipes. J. Hydraul. Res., *41*(5), 493–501.

Guo, J., and P. Y. Julien. 2008. Application of the modified log-wake law in open-channels. J. Appl. Fluid Mech., *1*(2), 17–23.

Guo, J., P. Y. Julien, and R. N. Meroney. 2005. Modified log-wake law in zero-pressure-gradient turbulent boundary layers. J. Hydraul. Res., *43*(4), 421–430.

Hinze, J. O. 1975. Turbulence, 2nd ed. New York: McGraw-Hill, 790 pp.

Howarth, M. J., and A. J. Souza. 2005. Reynolds stress observations in continental shelf seas. Deep Sea Res., Part II, *52*(9–10), 1075–1086.

Johnson, G. C., R. G. Lueck, and T. B. Sanford. 1994. Stress on the Mediterranean outflow plume: Part II. Turbulent dissipation and shear measurements. J. Phys. Oceanogr., *24*, 2084–2092.

Kang, S. K., M. G. G. Forman, H.-J. Lie, J.-H. Lee, J. Cherniawsky, and K.-D. Yum. 2002. Two-layer tidal modeling of the Yellow and East China Seas with application to seasonal variability of the M_2 tide. J. Geophys. Res.: Oceans, *107*(C3), 3020. doi: 10.1029/2001JC000838

Kim, S.-C., C. T. Friedrichs, J. P.-Y. Maa, and L. D. Wright. 2000. Estimating bottom stress in tidal boundary layer from acoustic Doppler velocimeter data. J. Hydraul. Eng., *126*(6), 399–406.

Lee, J. H., I. Lozovatsky, S.-T. Jang, C. J. Jang, C. S. Hong, and H. J. S. Fernando. 2006. Episodes of nonlinear internal waves in the northern East China Sea. Geophys. Res. Lett., *33*, L18601. doi: 10.1029/2006GL027136

Leo, L. S., Thompson, M., Di Sabatino, S., Fernando, H. J. S. 2015. Stratified flow past a hill: dividing streamline concept revisited. Bound. Layer Met. doi: 10.1007-s10546-105-101-1

Li, M. Z. 1994. Direct skin friction measurements and stress partitioning over movable sand ripples. J. Geophys. Res.: Oceans, *99*(C1), 791–799.

Long, R. R., and T.-C. Chen. 1981. Experimental evidence for the existence of the 'mesolayer' in turbulent systems. J. Fluid Mech., *105*, 19–59.

Lozovatsky, I., M. Figueroa, E. Roget, H. J. S. Fernando, and S. Shapovalov. 2005. Observations and scaling of the upper mixed layer in the North Atlantic. J. Geophys. Res.: Oceans, *110*, C05013. doi: 10.1029/2004JC002708

Lozovatsky, I., Z. Liu, H. Fernando, J. Armengol, and E. Roget. 2012. Shallow water tidal currents in close proximity to the seafloor and boundary-induced turbulence. Ocean Dyn., *62*, 177–191.

Lozovatsky, I., Z. Liu, H. Wei, and H. J. S. Fernando. 2008a. Tides and mixing in the northwestern East China Sea, Part I: Rotating and reversing tidal flows. Cont. Shelf Res., *28*(2), 318–337.

Lozovatsky, I., Z. Liu, H. Wei., and H. J. S. Fernando. 2008b. Tides and mixing in the northwestern East China Sea, Part II: Near-bottom turbulence. Cont. Shelf Res., *28*(2), 338–350.

Lozovatsky, I. D., E. Roget, H. J. S. Fernando, M. Figueroa, and S. Shapovalov. 2006. Sheared turbulence in a weakly stratified upper ocean. Deep Sea Res., Part I, *53*, 387–407.

Lozovatsky, I., E. Roget, J. Planella, H. J. S. Fernando, and Z. Liu. 2010. Intermittency of near-bottom turbulence in tidal flow on a shallow shelf. J. Geophys. Res.: Oceans, *115*, C05006. doi: 10.1029/2009JC005325

Lu, Y., and R. G. Lueck. 1999a. Using a broadband ADCP in a tidal channel. Part I: Mean flow and shear. J. Atmos. Oceanic Technol., *16*, 1556–1567.

Lu, Y., and R. G. Lueck. 1999b. Using a broadband ADCP in a tidal channel. Part II: Turbulence. J. Atmos. Oceanic Technol., *16*, 1568–1579.

Ludwick, J. C. 1975. Variations in the boundary-drag coefficient in the tidal entrance to Chesapeake Bay, Virginia. Mar. Geol., *19*, 19–28.

Lueck, R. G., and Y. Lu. 1997. The logarithmic layer in a tidal channel. Cont. Shelf Res., *17*, 1785–1801.

Matsuno, T., M. Shimizu, Y. Morii, H. Nishida, and Y. Takaki. 2005. Measurements of the turbulent energy dissipation rate around the shelf break in the East China Sea. J. Oceanogr., *61*(6), 1029–1037.

Munk, W. H., and E. R. Anderson. 1948. Notes on the theory of the thermocline. J. Mar. Res., *7*(3), 276–295.

Perlin, A., J. N. Moum, and J. M. Klymak. 2005. Response of the bottom boundary layer over a sloping shelf to variations in alongshore wind. J. Geophys. Res.: Oceans, *110*, C10S09. doi: 10.1029/2004JC002500

Perlin, A., J. N. Moum, J. M. Klymak, M. D. Levine, T. Boyd, and P. M. Kosro. 2005. A modified law-of-the-wall applied to oceanic bottom boundary layers. J. Geophys. Res.: Oceans, *110*, C10S10. doi: 10.1029/2004JC002310

Perlin, A., J. N. Moum, J. M. Klymak, M. D. Levine, T. Boyd, and P. M. Kosro. 2007. Organization of stratification, turbulence, and veering in bottom Ekman layers. J. Geophys. Res.: Oceans, *112*, C05S90. doi: 10.1029/2004JC002641

Pollard, R. T., P. B. Rhines, and R. O. R. Y. Thompson. 1972. The deepening of the wind-mixed layer. Geophys. Fluid Dyn., *4*(1), 381–404.

Rippeth, T. P. 2005. Mixing in seasonally stratified shelf seas: A shifting paradigm. Philos. Trans. R. Soc., A, *363*, 2837–2854.

Roget, E., I. Lozovatsky, X. Sanchez, and M. Figueroa. 2006. Microstructure measurements in natural waters: Methodology and applications. Prog. Oceanogr., *70*(2–4), 126–148.

Sakamoto, K., and K. Akitomo. 2008. The tidally induced bottom boundary layer in a rotating frame: Similarity of turbulence. J. Fluid Mech., *615*, 1–25.

Sanford, T. B., and R.-C. Lien. 1999. Turbulent properties in a homogeneous tidal bottom boundary layer. J. Geophys. Res.: Oceans, *104*(C1), 1245–1257.

Schlichting, H. 1968. Boundary-Layer Theory, 6th ed. New York: McGraw-Hill, 747 pp.

Smith, J. D., and S. R. McLean. 1977. Spatially averaged flow over a wavy surface. J. Geophys. Res., *82*, 1735–1746.

Souza, A., and C. Friedrichs. 2005. Near-bottom boundary layers, *in* Marine Turbulence: Theories, Models, and Observations, Results of the CARTUM Project, H. Baumert, J. H. Simpson, and J. Sündermann, eds. New York: Cambridge University Press, 283–296.

Souza, A. J., and M. J. Howarth. 2005. Estimates of Reynolds stress in a highly energetic shelf sea. Ocean Dyn., *55*, 490–498.

Stacey, M. T., S. G. Monismith, and J. R. Burau. 1999. Measurements of Reynolds stress profiles in unstratified tidal flow. J. Geophys. Res.: Oceans, *104*(C5), 10933–10949.

Sternberg, R. W. 1968. Friction factors in tidal channels with differing bed roughness. Mar. Geol., *6*, 243–260.

Thorpe, S. A. 2005. The Turbulent Ocean. Cambridge: Cambridge University Press, 439 pp.

Trowbridge, J. H., and S. J. Lentz. 1991. Asymmetric behavior of an oceanic boundary layer above a slopping bottom. J. Phys. Oceanogr., *21*, 1171–1185.

van Haren, H., N. Oakey, and C. Garrett. 1994. Measurements of internal wave band eddy fluxes above a sloping bottom. J. Mar. Res., *52*, 909–946.

Walter, R. K., M. E. Squibb, C. B. Woodson, J. R. Koseff, and S. G. Monismith. 2014. Stratified turbulence in the nearshore coastal ocean: dynamics and evolution in the presence of internal bores. J. Geophys. Res. Oceans, *119*, 8709–8730. doi: 10.1002/2014JC010396

Weatherly, G. L., and P. J. Martin. 1978. On the structure and dynamics of the oceanic bottom boundary layer. J. Phys. Oceanogr., *8*, 557–570.

Wimbush, M., and W. Munk. 1970. The benthic boundary layer, *in* The Sea, Vol. 4, New Concepts of Sea Floor Evolution, Part 1, A. E. Maxwell, ed. New York: Wiley, 731–758.

Wolk, F., H. Yamazaki, L. Seuront, and R. G. Lueck. 2002. A new free-fall profiler for measuring biophysical microstructure. J. Atmos. Oceanic Technol., *19*, 780–793.

Yoshikawa, Y., T. Endoh, T. Matsuno, T. Wagawa, E. Tsutsumi, H. Yoshimura, and Y. Morii. 2010. Turbulent bottom Ekman boundary layer measured over a continental shelf. Geophys. Res. Lett., *37*, L15605. doi: 10.1029/2010GL044156

Zilitinkevich, S. S. 1972. On the determination of the height of the Ekman boundary layer. Boundary-Layer Meteorol., *3*, 141–145.

Zilitinkevich, S. S., and I. N. Esau. 2002. On integral measures of the neutral barotropic planetary boundary layer. Boundary-Layer Meteorol., *104*, 371–379.

Received: *11 January 2015*; revised: *22 July 2015*.